Extended Data Figures

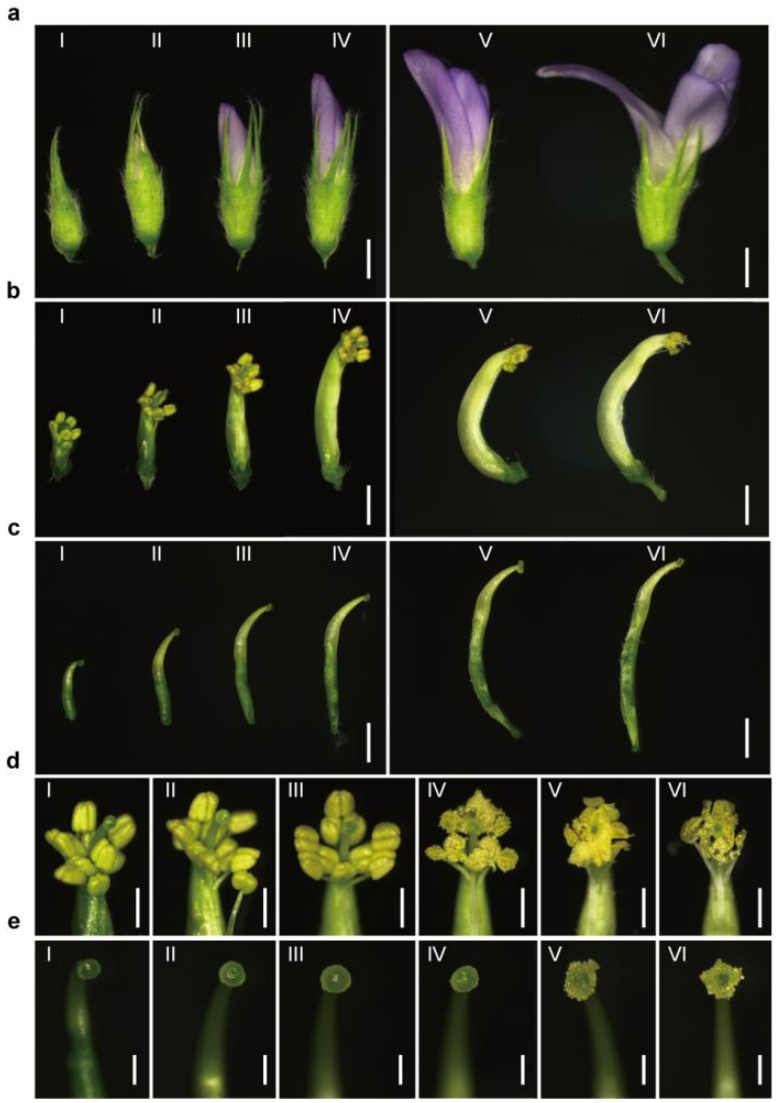

Extended Data Fig. 1 | Developmental stages of alfalfa flower and floral organs. a, Intact flower. **b**, Sexual column, a structure with the staminal column surrounding the pistil. **c**, Pistil. Scale bars, 1 mm. **d**, Diadelphous stamens and pistils. **e**, Close-up of stigma. Six distinct developmental stages (I-VI) were designated. Scale bars, 500 μm.

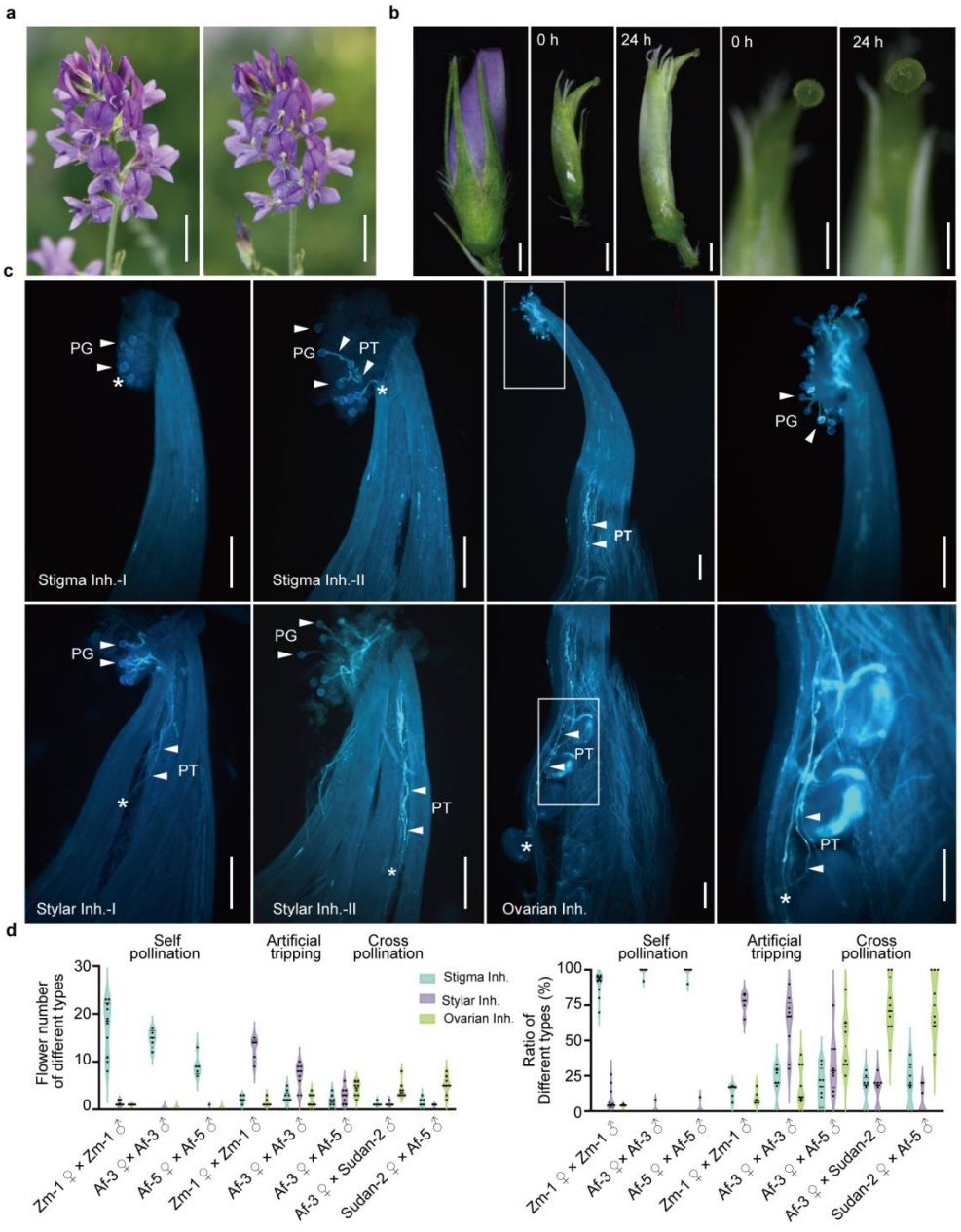

Extended Data Fig. 2 | Multi-layered barriers inhibiting self-pollen tube growth in alfalfa. a, Self-pollination after artificial tripping at Stage VI. Left and Right: Flowers before and after artificial tripping. Scale bars, 1 cm. **b**, Cross-pollination at Stage III. **c**, In self-pollination, pollen tube growth is blocked at the surface of stigma (stigma inh.). Artificial tripping partially bypasses this barrier, allowing limited pollen tubes to grow into the style but arrested therein (stylar inh.). In contrast, cross-pollination enables compatible interactions and some pollen tubes elongating successfully to the ovules, whereas some others arrested in ovary (ovarian inh.). Scale bars, 200 μm. **d**, Number of flowers assessed per treatment (left), and ratio of

different pollen tube inhibitions observed in self- vs. cross-pollinated flowers (right). White arrowheads point to pollen grains or pollen tubes.

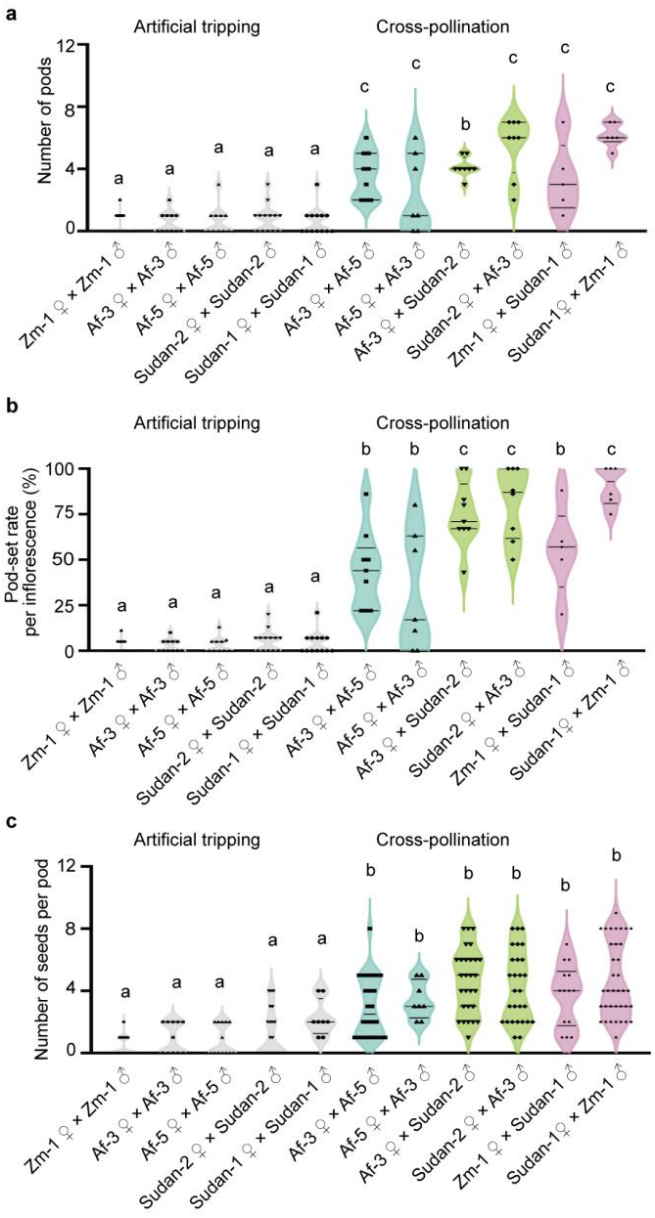

Extended Data Fig. 3 | Pod and seed set in alfalfa after self- and cross-pollination. **a**, Number of pods formed per flower. **b**, Pod set rate per inflorescence. **c**, Number of seeds per pod. Artificial self-pollination reduces pod formation and seed yield, cross-pollination significantly increases both pod and seed production. Different letters were assigned to the means based on a significant difference at the probability level of $p < 0.001$ as determined by Tukey's multiple range test.

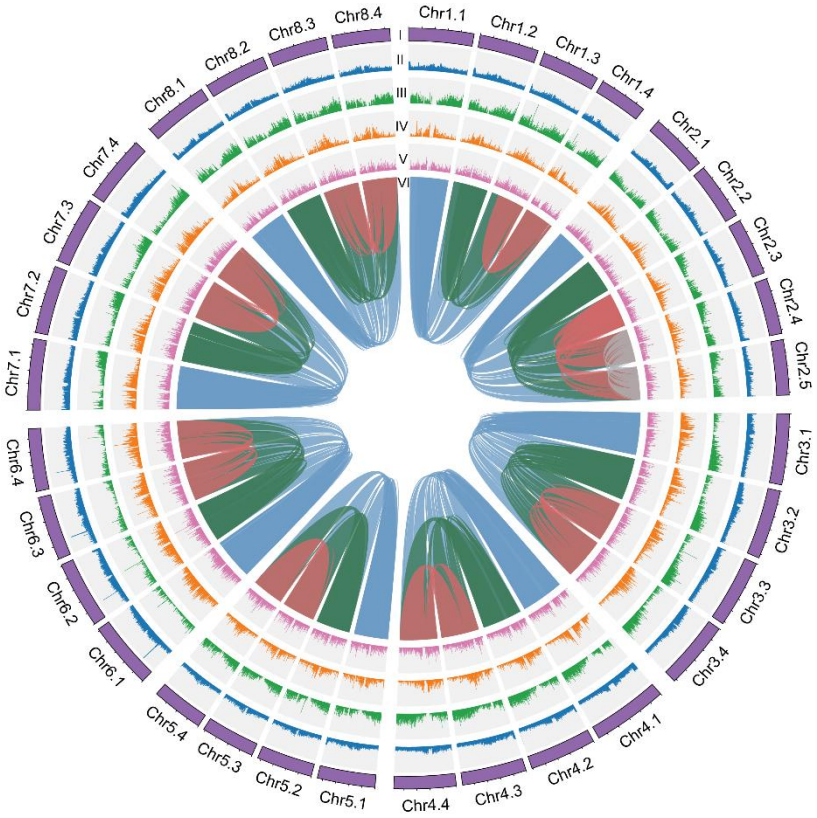

Extended Data Fig. 4 | Circos plot of the phased genome assembly of *M. sativa* cv. Zhongmu-1. Tracks from outermost to innermost: (I) chromosomes, (II) GC content, (III) gene density, (IV) Gypsy density, (V) Copia density, and (VI) intra-genomic syntenic blocks. Chr2.5 indicates an extra chromosome 2.

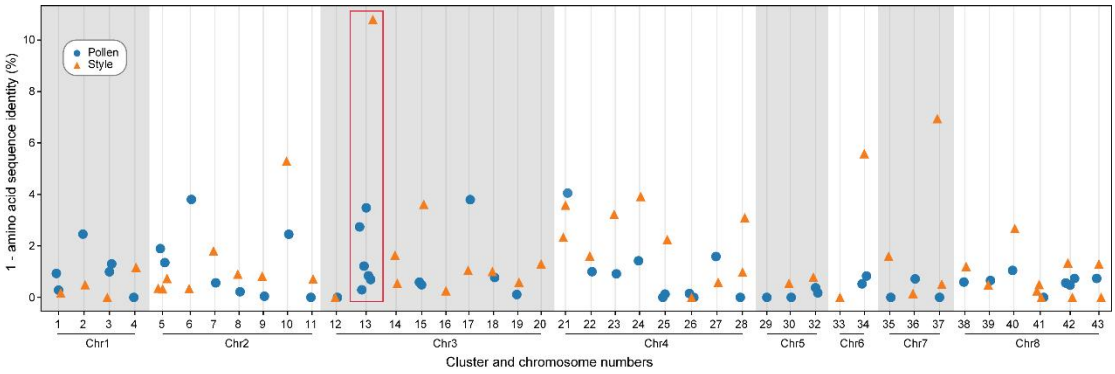

Extended Data Fig. 5 | Protein sequence polymorphisms of pollen- and pistil-specific alleles within the clusters. Blue dots represent pollen-expressed proteins, and orange triangles represent pistil-expressed proteins. Horizontal lines under the X axis indicate the cluster IDs and their corresponding chromosomal locations. The Y axis indicates amino acid polymorphisms expressed as 1-amino acid sequence identity in percentage.

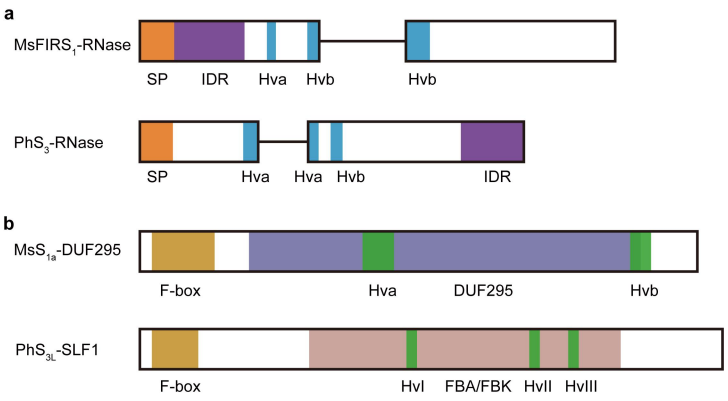

Extended Data Fig. 6 | Gene structures and annotated protein domains of *S* genes in alfalfa and petunia. a, Gene structure and protein domain organizations of the pistil *S* genes *MsFIRS1-RNase* from alfalfa and *PhS3-RNase* from petunia, respectively. **b,** Gene structure and protein domain organizations of the pollen *S* genes *MsS1a-DUF295* from alfalfa and *PhS3L-SLF1* from petunia, respectively.

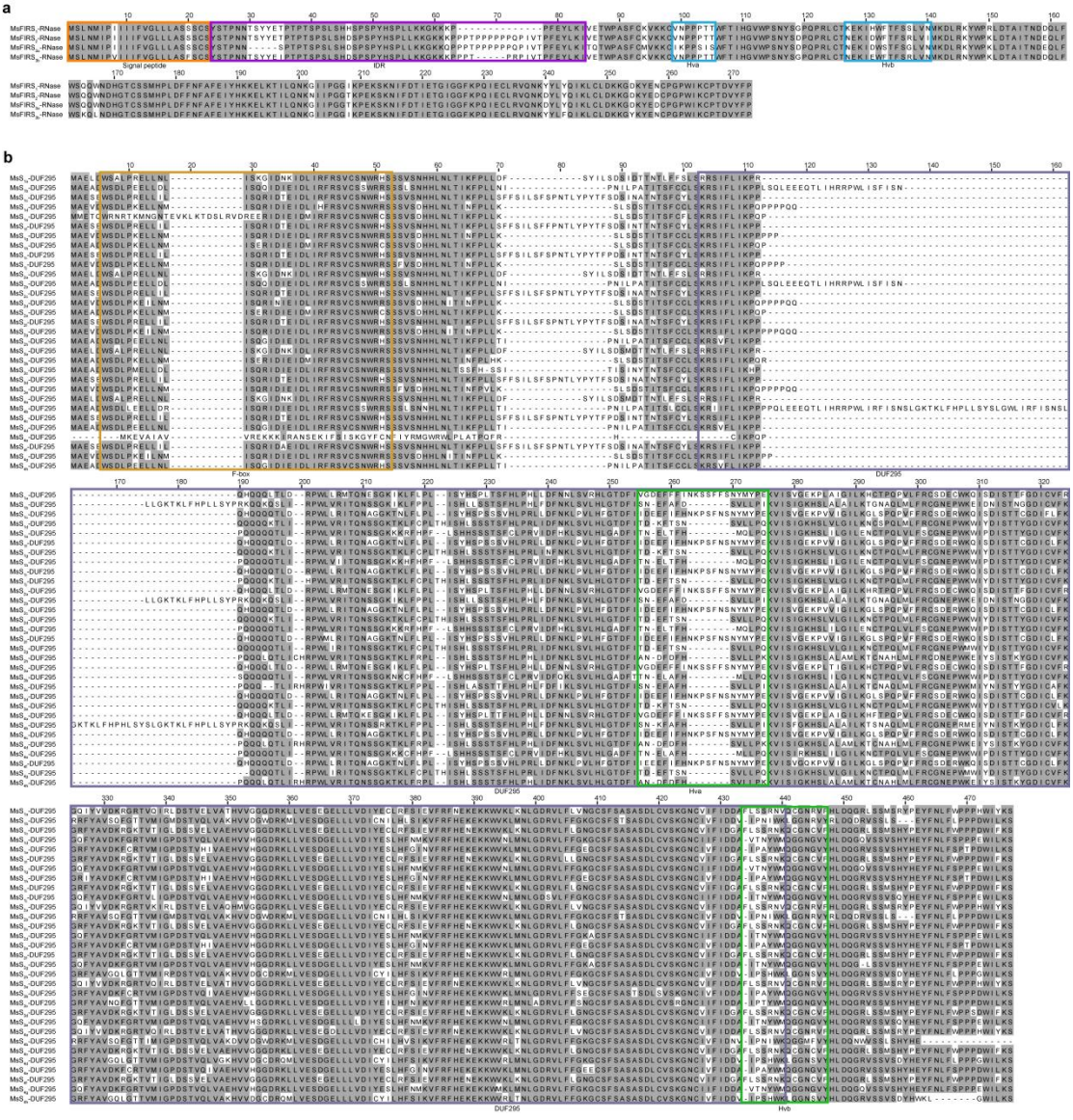

Extended Data Fig. 7 | Protein sequence alignments of *S* genes in *M. sativa* cv. Zhongmu-1. a, Multiple sequence alignment of FIRS-RNase proteins. **b,** Multiple sequence alignment of S-DUF295 proteins. Different domains are color boxed.

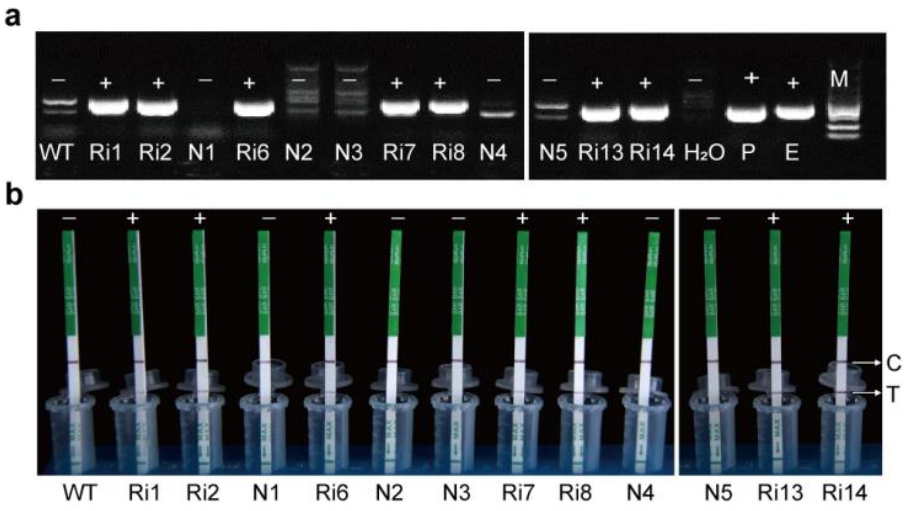

Extended Data Fig. 8 | Molecular identification of transgenic alfalfa RNAi lines of *MsFIRS$_{3b}$-RNase*. **a**, PCR amplification of the specific vector fragment from genomic DNA of putative transgenic lines. Lanes: E, *Agrobacterium tumefaciens* strain EHA105 harboring the plasmid; P, plasmid vector (positive control); M, DNA molecular weight marker. **b**, Detection of the BAR selectable marker protein using an immunochromatographic lateral flow assay. White arrows indicate the control (C) and test (T) lines, positive result was interpreted when both the C and T lines were clearly visible. '+' or '-' indicate transgenic positive and non-transgenic negative controls.

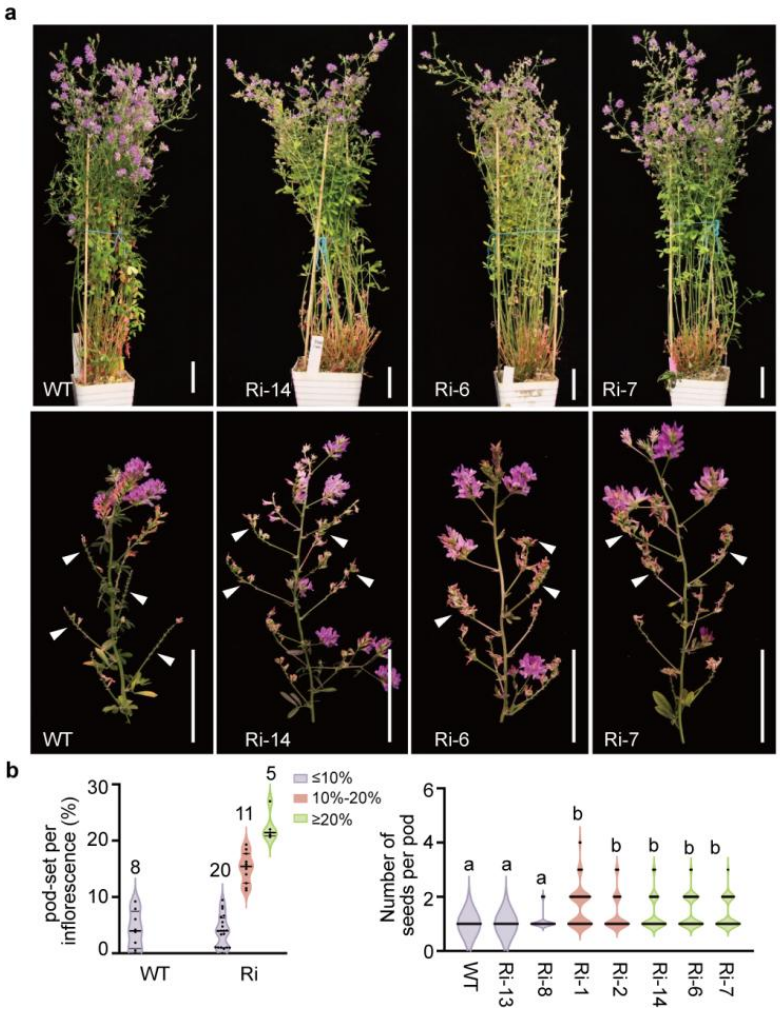

Extended Data Fig. 9 | RNAi-mediated suppression of *MsFIRS$_{3b}$-RNase* significantly enhances fertility in the transgenic alfalfa lines. a, Compared to non-transgenic controls, *MsFIRS$_{3b}$-RNase* RNAi transgenic lines exhibited no obvious morphological alterations (Top), but displayed a significant increase in fertility (Bottom). Scale bars, 15 cm. **b**, Quantification of the distribution of pod set rates for individual transgenic and non-transgenic lines. Left: Pod set rates were categorized into the three ranges: ≤10%, 10-20% and ≥20%. Numbers above bars indicate the plant count (n) in each category. Right: Number of seeds per pod.

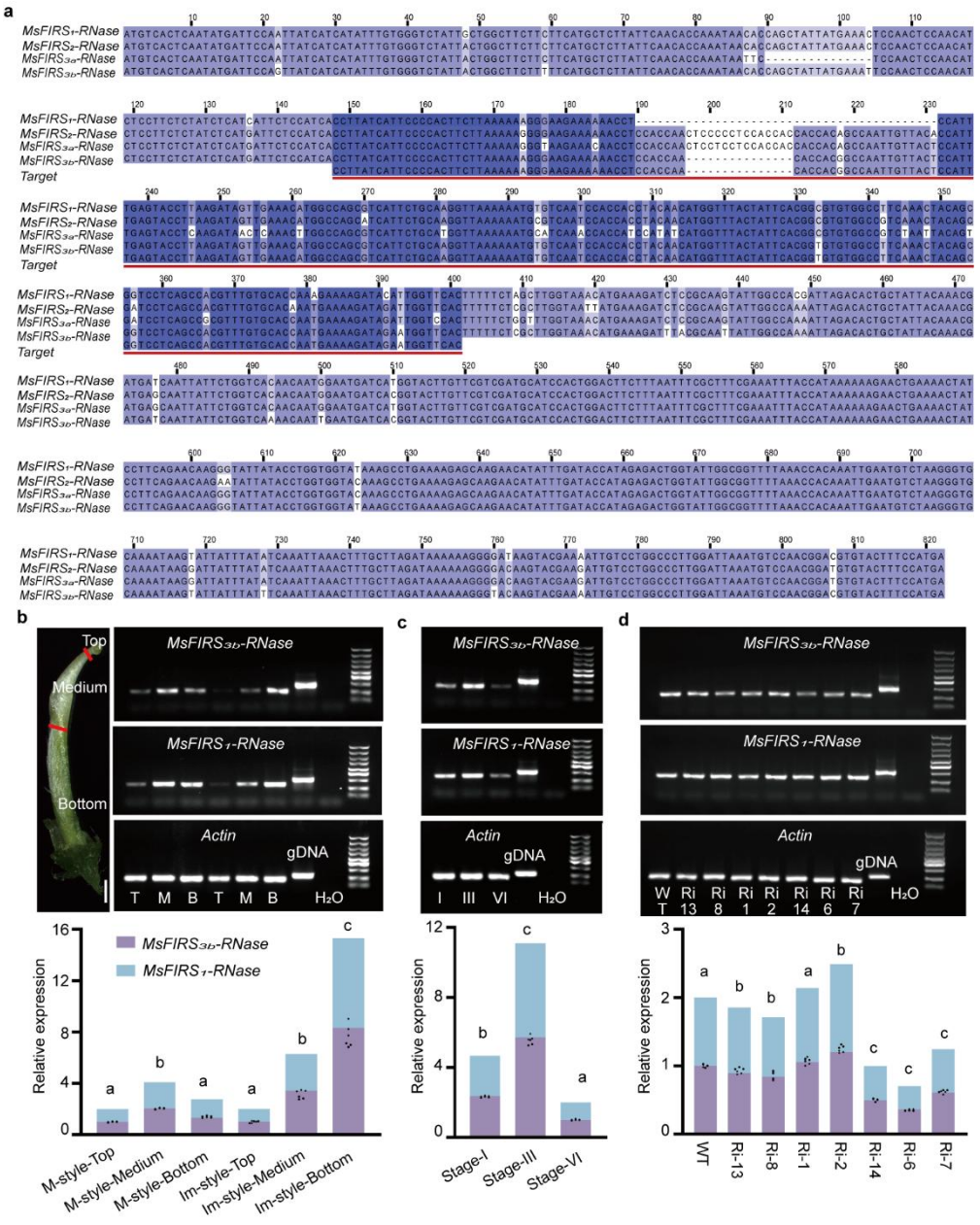

Extended Data Fig. 10 | Spatiotemporal expression pattern of *MsFIRS$_1$-RNase* and *MsFIRS$_{3b}$-RNase*. **a**, Multiple sequence alignment of *MsFIRS-RNase*s and the RNAi target sequence. The target RNAi sequence is highlighted with a red underline. **b**, *MsFIRS-RNase*s exhibit spatiotemporal expression gradient along the style (T, stigma; M, style transmitting tract; B, ovary), and this expression pattern differs significantly between mature (M-style) and immature (Im-style) pistils. Scale bars, 500 μm. **c**, Temporal expression of *MsFIRS-RNase*s during different development stages I, III, and VI. **d**, *MsFIRS-RNase* expression is down-regulated in highly fertile RNAi transgenic lines (e.g., lines Ri-6, Ri-7, and Ri-14). The upper panel shows

RT-PCR results, the lower panel shows quantitative real-time PCR (qPCR) results from three technical replicates. Data are presented as mean ± SD. Different letters indicate significant differences at $p < 0.01$ according to Duncan's multiple range test.

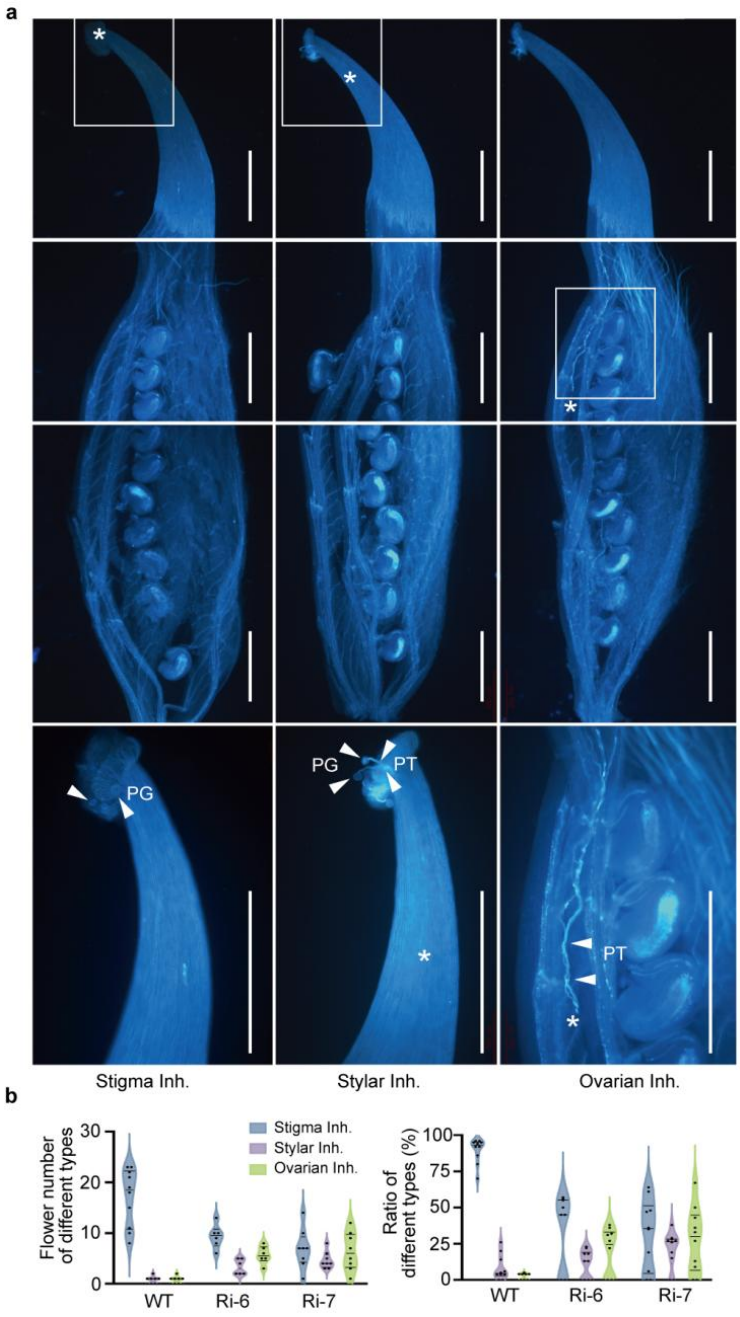

Extended Data Fig. 11 | Comparison of pollen tube growth behaviors between the *MsFIRS$_{3b}$-RNase* RNAi transgenic lines and wild-type alfalfa.

a, Three distinct categories of pollen tube growth were observed: Pollen tubes arrested at the surface of stigma(stigma inh.), in the style (stylar. inh.), and in the ovary (ovarian inh.). The lower panel images are close-up of the white boxed areas in upper panels. Scale bars, 500 μm. **b**, Quantification of the number of flowers assessed for each treatment (left), and the ratio of pollen tube inhibition phenotypes (right).

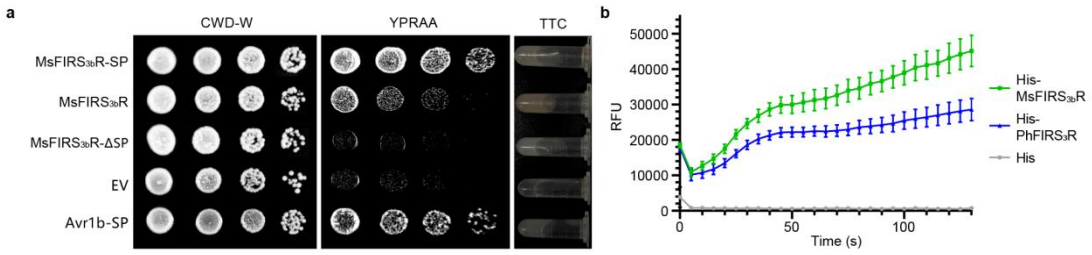

Extended Data Fig. 12 | MsFIRS$_{3b}$-RNase is a secreted ribonuclease. a, Functional validation of the signal peptide of MsFIRS$_{3b}$-RNase. CWD-W and YPRAA indicate media for the growth of yeast YTK12 strain carrying the signal peptide (SP) of MsFIRS$_{3b}$-RNase (MsFIRS$_{3b}$-RNase-SP), full-length coding sequence of MsFIRS$_{3b}$-RNase (MsFIRS$_{3b}$-RNase), MsFIRS$_{3b}$-RNase without SP (MsFIRS$_{3b}$-RNase-ΔSP), and the SP of Avr1b (Avr1b-SP) fused in frame to the invertase gene of the pSUC2 vector, respectively**.** TTC indicates whether the yeast can reduce 2,3,5-triphenyltetrazolium chloride (TTC) to an insoluble red-coloured compound (1,3,5-triphenylformazan, TPF). EV (empty pSUC2 vector) and Avr1b-SP represent negative and positive controls, respectively. **b**, Ribonuclease activity of His-MsS$_{3b}$-RNase indicated by relative fluorescence unit (RFU). The RFU during a time course indicated by the x axis is shown as mean ± s.e.m. (n = 3). His and His-tagged *Petunia hybrida* S$_3$-RNase (PhS$_3$-RNase) represent negative and positive control, respectively.

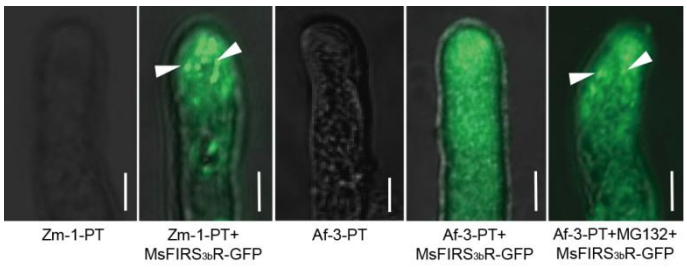

Extended Data Fig. 13 | MsFIRS$_{3b}$-RNase can enter both self and non-self pollen tubes of alfalfa. GFP fluorescence detection of recombinant MsFIRS$_{3b}$-RNase-GFP in self (Zm-1), non-self (Af-3), and MG132-treated non-self pollen tubes (PT) of alfalfa. Scale bars, 5 μm. White arrows point to the punctate structures.

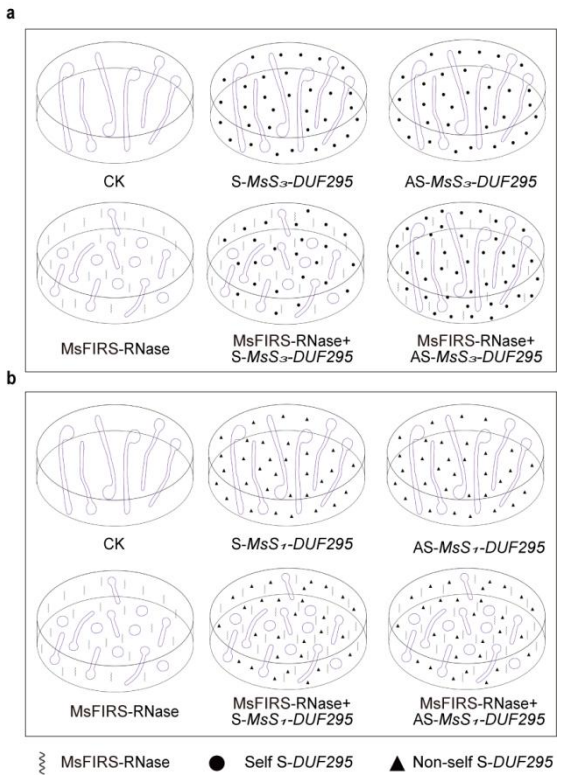

Extended Data Fig. 14 | Schematic representation of antisense oligonucleotide targeting *S-DUF295* action on alfalfa pollen tubes. a, Antisense oligonucleotide-mediated suppression of self *MsS$_3$-DUF295* alleviates MsFIRS-RNase inhibition of the pollen tube growth. **b,** In contrast, suppression of non-self *MsS$_1$-DUF295* fails to rescue the MsFIRS-RNase induced pollen tube growth inhibition.

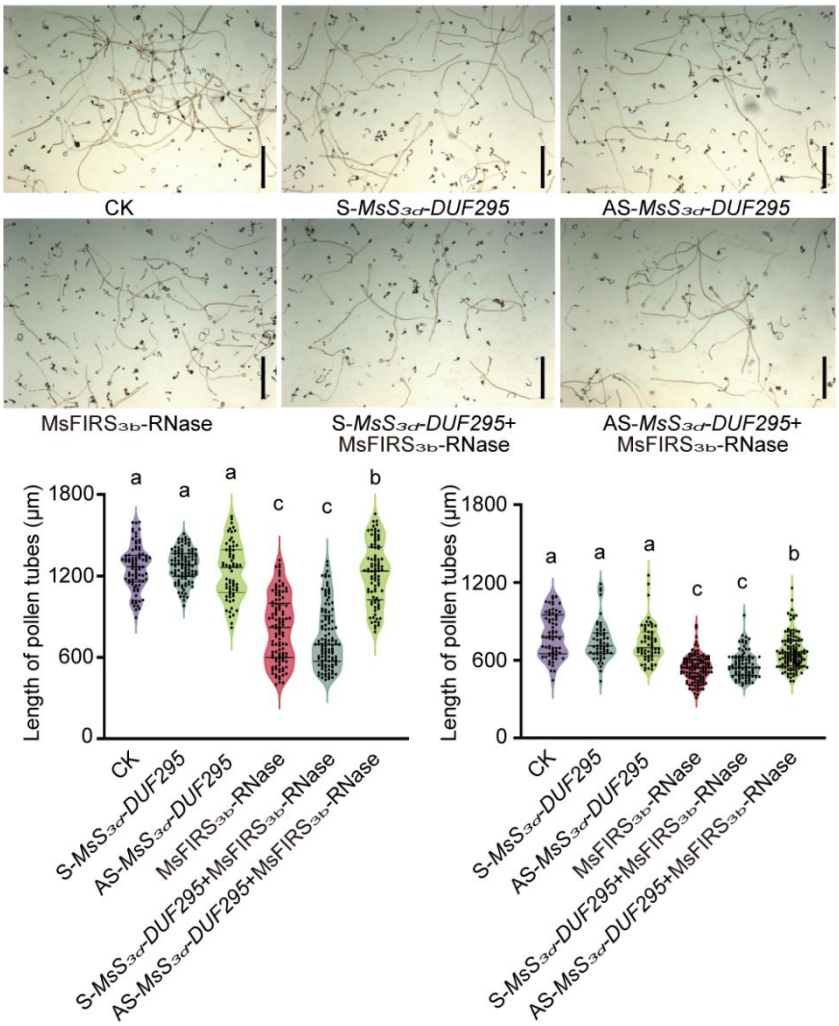

Extended Data Fig. 15 | Suppression of *MsS$_{3d}$-DUF295* by antisense oligonucleotides alleviates MsFIRS$_{3b}$-RNase mediated inhibition of the pollen tube growth. Top: Pollen tubes were incubated with MsFIRS$_{3b}$-RNase and 10 μM sense or antisense oligonucleotides targeting *MsS$_{3d}$-DUF295*. Bottom: Quantification of the pollen tube growth phenotypes after treatment with MsFIRS$_{3b}$-RNase at 50 μg/ml (left) and 150 μg/ml (right). Different letters were assigned to the means based on a significant difference at the probability level of $p < 0.001$ as determined by Tukey's multiple range test. Scale bars, 500 μm.

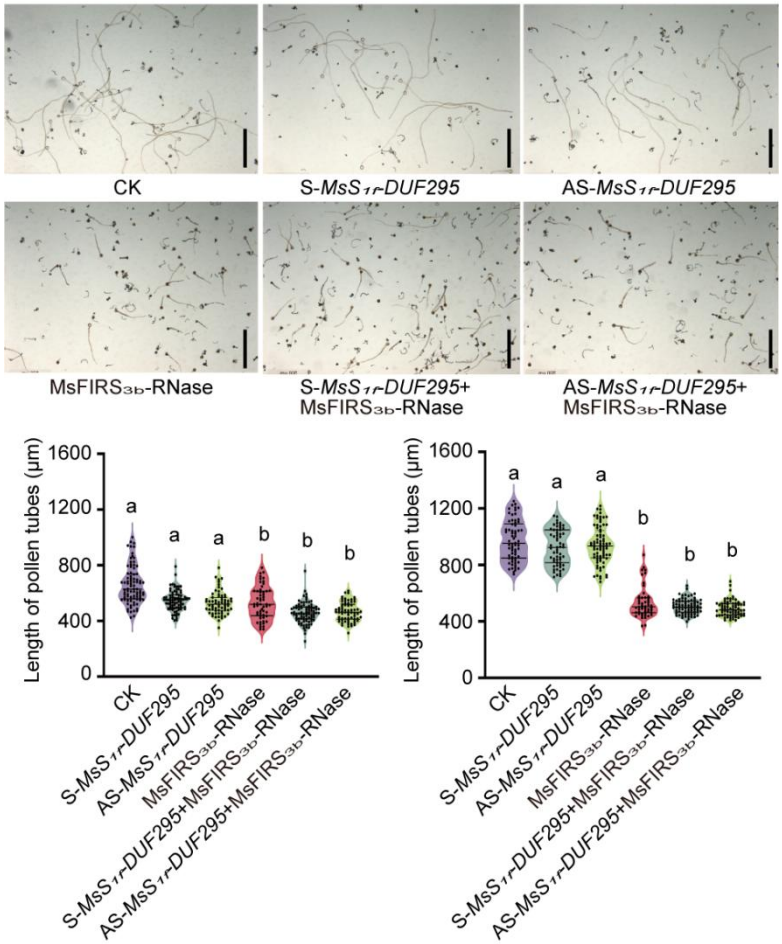

Extended Data Fig. 16 | Suppression of non-self *MsS$_{1f}$-DUF295* by antisense oligonucleotides does not rescue MsFIRS$_{3b}$-RNase induced pollen tube growth inhibition. Top: Antisense oligonucleotide targeting the non-self *MsS$_{1f}$-DUF295* fails to rescue FIRS-RNase-mediated toxicity. Bottom: Quantification of the pollen tube growth following treatment with 50 μg/ml (left) and 150 μg/ml (right) MsFIRS$_{3b}$-RNase. Different letters above the bars indicate significant differences ($p <$ 0.001) as determined by Tukey's multiple range test. Scale bars, 500 μm.

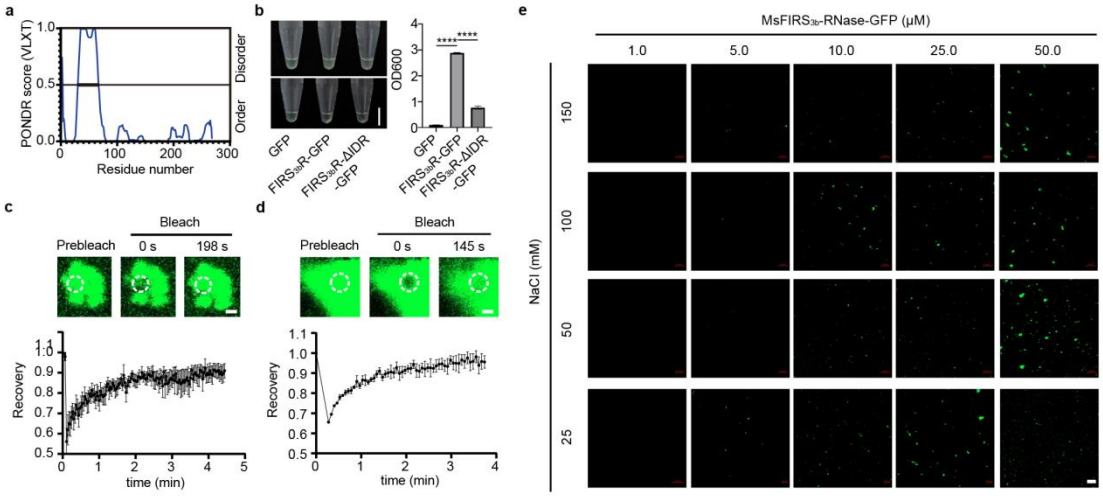

Extended Data Fig. 17 | MsFIRS$_{3b}$-RNase undergoes phase separation both *in vitro* and in *N. benthamiana* leaf cells. a, The intrinsically disordered regions of MsFIRS$_{3b}$-RNase predicted by PONDR (Predictor of Natural Disordered Regions). **b**, Turbidity detection of GFP, MsFIRS$_{3b}$-RNase-GFP, and MsFIRS$_{3b}$-RNase-ΔIDR-GFP. Left, visualization of the turbidity (top) and gelation state (bottom) of GFP, MsFIRS$_{3b}$-RNase-GFP, and MsFIRS$_{3b}$-RNase-ΔIDR-GFP. Scale bar, 1 cm. Right, Analyses of turbidity indicated by OD600 shown as mean ± s.e.m. (n = 3). ****, $p <$ 0.0001. **c**,**d**, Fluorescence recovery after photobleaching (FRAP) of MsFIRS$_{3b}$-RNase-GFP punctate structures *in vitro* (**c**) and in *N. benthamiana* leaf cells (**d**) with the curves indicating the time course of the recovery shown at the bottom. Scale bars, 10 μm. **e**, Confocal images showing the condensate dynamics of MsFIRS$_{3b}$-RNase-GFP at different protein and NaCl concentrations. Scale bar, 50 μm.

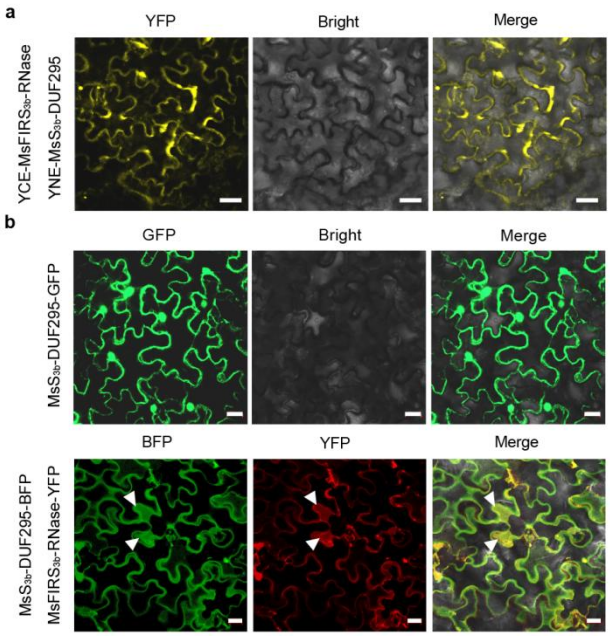

145

146 **Extended Data Fig. 18 | Interaction and co-localization between**

147 **MsFIRS$_{3b}$-RNase and MsS$_{3b}$-DUF295. a**, Interaction between MsFIRS$_{3b}$-RNase and

148 MsS$_{3b}$-DUF295 detected bimolecular fluorescence complementation (BiFC). YNE

149 and YCE, transiently expressed N- and C-terminal region of YFP, respectively. YFP,

150 Bright and Merge, the YFP fluorescence, bright and their merged field, respectively.

151 Scale bars, 20 μm. **b**, Subcellular localization of MsS$_{3b}$-DUF295 and the

152 co-localization of MsFIRS$_{3b}$-RNase and MsS$_{3b}$-DUF295 in *Nicotiana benthamiana*

153 leaf cells. Top, Subcellular localization of GFP-tagged MsS$_{2e}$-DUF295. GFP, Bright,

154 and Merge represent the GFP fluorescence, bright and their merged field, respectively.

155 Bottom, Co-localization of BFP-tagged MsS$_{3b}$-DUF295 with YFP-tagged

156 MsFIRS$_{3b}$-RNase in the plasmolyzed *N. benthamiana* leaf cells. White arrows point to

157 the florescent signals in the apoplast. Scale bars, 20 μm.

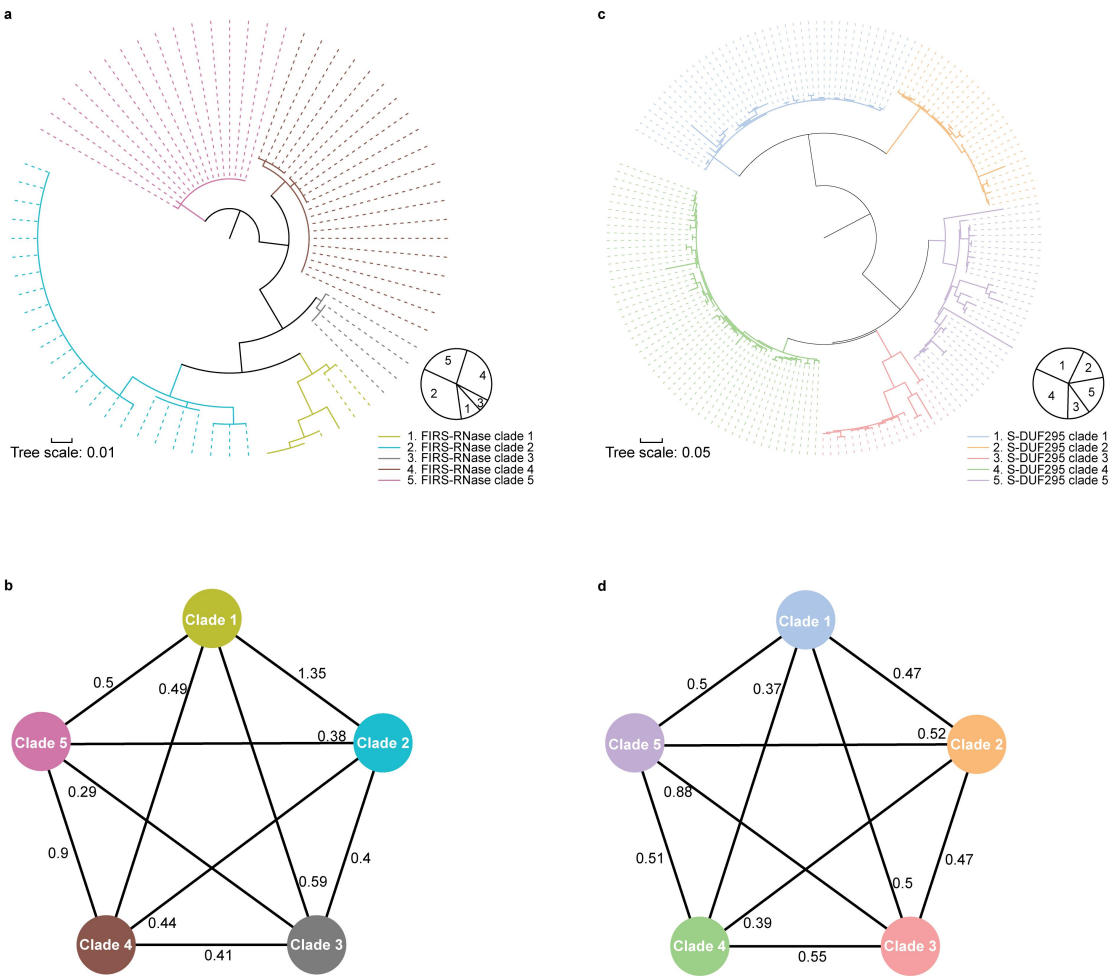

158

159 **Extended Data Fig. 19 | Phylogenetic relationships and *Ka*/*Ks* of *FIRS-RNase* and**

160 ***S-DUF295* genes. a**, Phylogenetic tree constructed based on *FIRS-RNase* protein

161 sequences. The five distinct clades are highlighted in different colors. **b**, The average

162 pairwise *Ka*/*Ks* values calculated between the different *FIRS-RNase* clades. **c**,

163 Phylogenetic tree of S-DUF295 protein sequences, with the five main branches

164 distinguished by different colors. **d**, The average inter-clade *Ka*/*Ks* values for

165 *S-DUF295* clades.

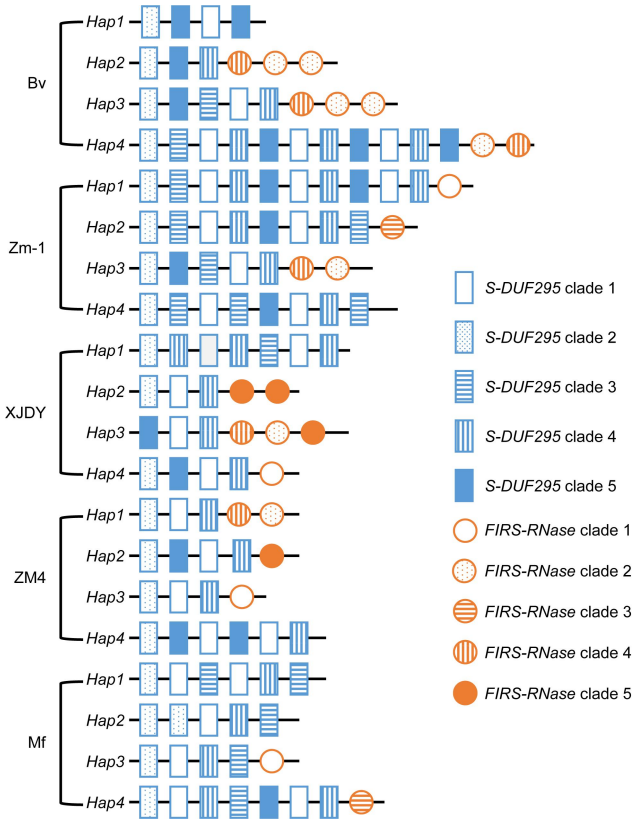

Extended Data Fig. 20 | Gene composition of the *S*-locus across haplotypes from five *M. sativa* accessions. The *S*-locus regions from Chromesome 3 haplotypes of *M.sativa* ssp. *sativa* Bolivia (Bv), Xinjiangdaye (XJDY), Zhongmu-1 (Zm-1), Zhongmu-4 (ZM4), and *M.sativa* ssp. *falcata* are shown. Genes are color-coded by type: *S-DUF295* (blue) and *FIRS-RNase* (orange). Within each gene type, distinct fill patterns correspond to the five major phylogenetic clades identified in Extended Data Figure 19.